Characterization and Localization of Partial-Discharge-Induced Pulses in Fission Chambers Designed for Sodium-Cooled Fast Reactors

Giacomo Galli, Hassen Hamrita, C. Jammes, Michael J Kirkpatrick, E. Odic, Philippe Dessante, Philippe Molinié, B. Cantonnet, J.-C. Nappé

Characterization and Localization of Partial-Discharge-Induced Pulses in Fission Chambers Designed for Sodium-Cooled Fast Reactors

G. Galli , H. Hamrita, C. Jammes, M. J. Kirkpatrick, E. Odic, Ph. Dessante, Ph. Molinie, B. Cantonnet, and J.-C. Nappé

Abstract— **During the operation of the superphenix and phenix reactors, an aberrant electrical signal was detected from the fission chambers used for neutron flux monitoring. This signal, thought to be due to partial electrical discharge (PD) is similar to the signal resulting from neutron interactions, and is generated in fission chambers at temperatures above 400 °C. This paper reports work on the characterization and localization of the source of this electrical signal in a high-temperature fission chamber. The dependence of the shape of the PD or neutron signal on the various experimental parameters (nature and pressure of the chamber filling gas, electrode gap distance, and fission chamber geometry) are described. Next, experiments designed to identify the location within the chambers where the PD are being generated are presented in way to propose changes to the fission chamber in order to reduce or eliminate the PD signal.**

Index Terms— **Fission chamber, high temperature, neutron detector, partial discharge (PD), sodium-cooled fast reactors, triple point effect.**

I. Introduction

A PROMINENT application of high-temperature fission chambers (HTFC) [1] is to detect neutrons inside the core of sodium-cooled fast reactors [2]–[10]. Multiple uses are envisaged such as reactor power control and fuel cladding failure detection [11], [12].To operate in core, the HTFC will have to withstand the high operating temperatures, up to 650 °C, of the sodium-cooled fast reactors and also to operate under high irradiation, up to 10^{10} n/cm$^2 \cdot$ s.

After years of study [7]–[10], it is now known that an electrical signal, here referred to as a partial discharge (PD), more or less similar to the signal resulting from neutron interactions, is generated in fission chambers at temperatures above 400 °C.

This unwanted signal poses challenges, especially during reactor startup when the PD signal count may be on the same order of magnitude as the neutron signal count [10]. In addition to problems with reactor startup, the unwanted signal will prohibit fuel clad failure detection, which relies on a very precise neutron count in the sodium coolant circulation lines.

The study presented in this paper aims to characterize this PD signal compared with the signal resulting from neutron detection, and to locate the problematic zone of the chamber.

A brief summary of electrical discharge theory is described in Section II. The fission chambers and the experimental setup used in this paper are described, respectively, in Sections III and IV. All results on the pulse shape characterization are presented in Section V. All results on PD localization and a brief overview of the methods used are presented in Section VI.

II. Theoretical Concepts of Electric Discharge Theory

Electrical discharge can occur when a seed electron is accelerated by an imposed electric field, acquiring energy superior to the ionization energy of the gas atoms/molecules, and leading to an electron avalanche. Sources of seed electrons include cosmic rays and photoionization.

The schematic shown in Fig. 1 describes the basic process of an electronic discharge in a plane to plane geometry. Assuming the presence of a seed electron, the conditions which will lead to an electron avalanche are described by Paschen's law [24]–[26]

$$V = \frac{B \times P \times d}{\ln\left(A \times P \times d\right) - \ln\left(\ln\left(1 + \frac{1}{\gamma}\right)\right)} \tag{1}$$

Manuscript received April 25, 2018; accepted July 26, 2018. Date of publication July 31, 2018; date of current version September 14, 2018. This work was supported by the CEA, the French Alternative Energies and Atomic Energy Commission.

G. Galli is with the Sensors and Electronic Architectures Laboratory, CEA, LIST, 91192 Gif-sur-Yvette, France, with the Group of Electrical Engineering, UMR CNRS 8507, 91192 Gif-sur-Yvette, France, with CentraleSupélec, Université Paris-Sud, Université Paris-Saclay, Sorbonne Universités, 91192 Gif-sur-Yvette, France, and also with UPMC Université Paris 06, 3 & 11 rue Joliot-Curie, Sorbonne Universités, 91192 Gif-sur-Yvette CEDEX, France (e-mail: giacomo.galli@cea.fr).

H. Hamrita is with the Sensors and Electronic Architectures Laboratory, CEA, LIST, 91192 Gif-sur-Yvette, France.

C. Jammes is with the Instrumentation, Sensors and Dosimetry Laboratory, CEA, DEN, DER, 13115 Saint-Paul-lez-Durance, France.

M. J. Kirkpatrick, E. Odic, Ph. Dessante, and Ph. Molinie are with the Group of Electrical Engineering, UMR CNRS 8507, 91192 Gif-sur-Yvette, France, with CentraleSupélec, Université Paris-Sud, Université Paris-Saclay, Sorbonne Universités, 91192 Gif-sur-Yvette, France, and also with UPMC Université Paris 06, 3 & 11 rue Joliot-Curie, Sorbonne Universités, 91192 Gif-sur-Yvette, France.

B. Cantonnet and J.-C. Nappé are with PHOTONIS France, Nuclear Instrumentation, 19100 Brive la gaillarde, France.

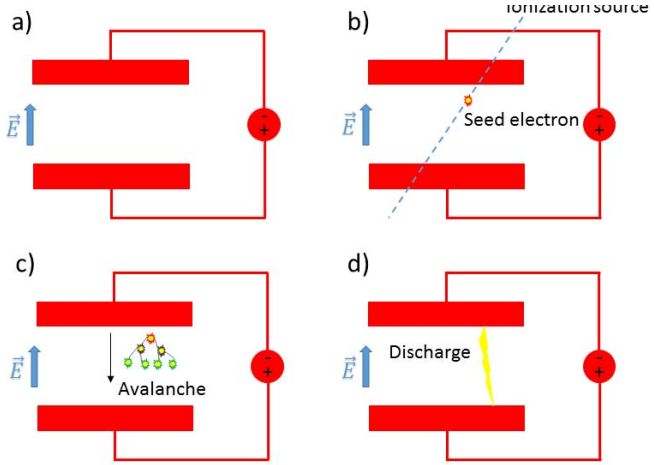

Fig. 1. Electric discharge scheme in a plane to plane geometry.

TABLE I
PASCHEN LAW EMPIRICAL COEFFICIENTS [22]

	A (Torr^{-1}cm^{-1})	B (V Torr^{-1}cm^{-1})
H_2	5	130
N_2	12	342
Air	15	365
He	3	34
Ne	4	100
Ar	14	180
Xe	26	350

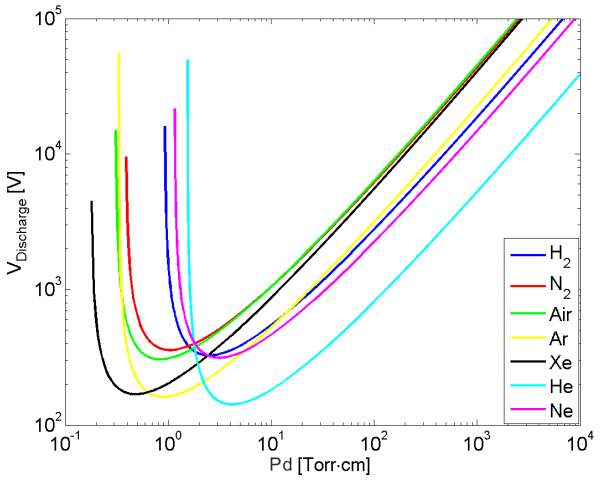

Fig. 2. Paschen curve for different gasses.

where P and d are the filling gas pressure and the interelectrode distance, γ is the secondary emission coefficient (the yield of electrons from positive ion impact on the cathode which is normally on the order of 10^{-4}–10^{-2}), and A and B are coefficients which depend on the gas nature and are tabulated, for the main gases, in Table I.

Fig. 2 shows Paschen curves for different gases. The abscissa is the product of the pressure times the interelectrode distance, and the ordinate is the voltage above which a discharge could occur. The discharge voltage passes by a minimum value on the order of a few hundred volts, depending on gas type.

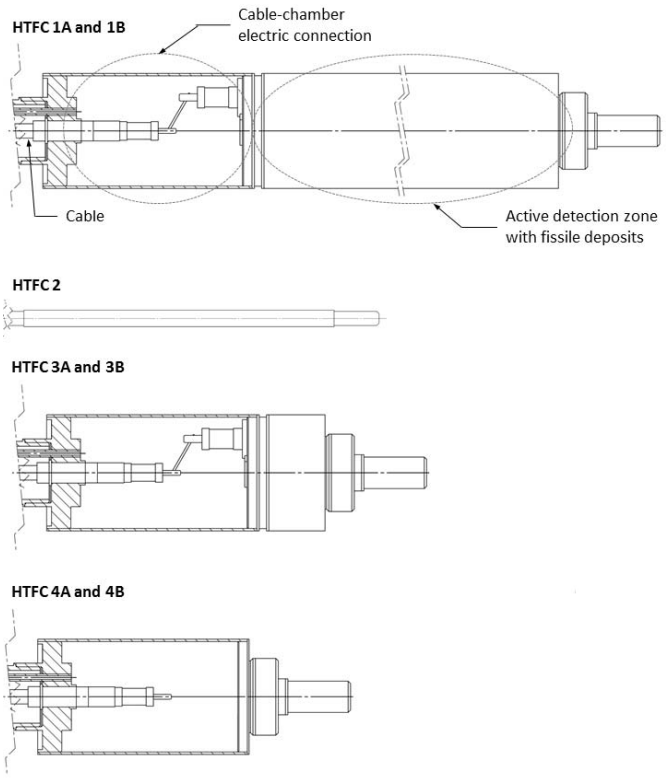

Fig. 3. Drawings of HTFCs manufactured by PHOTONIS and used in this paper.

Paschen's law is derived for a case of infinite planar electrodes, in other words, for the case of a homogeneous electric field. This is of course different from the case of a fission chamber, especially from the point of view that, in a fission chamber, the electrodes are held in place and electrically insulated from each other by a ceramic insulating component. The presence of the insulating ceramic material, which may become electrically charged, and whose dielectric properties are dependent on the temperature, is likely an important aspect of this type of system. In addition, the complex geometry of the system in combination with the presence of the ceramic insulator produces inhomogeneities of the electric field.

III. DESCRIPTION OF THE FISSION CHAMBERS

Fig. 3 shows both the full and partial fission chambers used in this paper; all these chambers were manufactured by PHOTONIS France using the same processes.

A full fission chamber consists of an active zone with cylindrical electrodes covered in fissile material, and a zone which serves to assure the electrical connection between the active zone and the cable which conducts signals to an amplifier. This means that there are two electrical connections in a complete chamber. The first two complete fission chambers (HTFC 1A and 1B), whose parameters are shown in Table II, both have the geometry shown in Fig. 3, but are filled with argon to two different pressures. The third complete fission chamber (HTFC 2) listed in Table II is the chamber with the smaller diameter depicted in Fig. 3.

TABLE II
HTFCs Parameters

	Diameter [mm]	Electrodes distance [mm]	Bias Voltage [Volt]	Gas Pressure [bar]	N. electrodes
HTFC 1A	48	1.5	400	1.5	3
HTFC 1B	48	1.5	400	3.5	3
HTFC 2	7.0	0.5	200	9.0	2
HTFC 3A	48	--	400	1.5	--
HTFC 3B	48	--	400	3.5	--
HTFC 4A	48	--	400	1.5	--
HTFC 4B	48	--	400	3.5	--

TABLE III
Mean Values and Standard Deviations of Neutrons Pulses FWHM

		μ[ns]	σ[ns]
HTFC 1A	(20°C ; 400V)	119	30
	(650°C ; 400V)	154	95
HTFC 1B	(20°C ; 400V)	102	25
	(500°C ; 400V)	125	79
	(650°C ; 400V)	134	55
HTFC 2	(20°C ; 200V)	98	24
	(500°C ; 200V)	123	69

The last four chambers (HTFC 3A, HTFC 3B, HTFC 4A, and HTFC 4B) listed in Table II are partial chambers, having no active zone but containing either both or only one of the aforementioned electrical connectors as shown in Fig. 3; these chambers were also prepared with two different filling gas pressures, as shown in Table II.

All of the chambers were filled with pure argon (purity level of 99.9999%) and the complete chambers (HTFC 1A, HTFC 1B, and HTFC 2) were initially tested at room temperature and in the presence of neutron flux to ensure their proper operation under standard conditions [8].

After these tests, all fission chambers were heated to different temperatures and electrically polarized in order to observe the appearance of PDs.

IV. Experimental Setup

All chambers shown in Fig. 3 are tested using the same measurement chain, they are tested in three different conditions: at room temperature with a neutron source, with a high-temperature environment but without any neutron source and with neutron source and temperature at the same time.

All the experiments shown in this paper was carried out in a ground level laboratory, without any radiation shield, and in underground level shielded laboratory calls Saphir facility [14]–[18]. The Saphir facility is a linear electron accelerator which, in our experiments, accelerates a bench of electrons at mean energy of 18 MeV, every 20 ms, to a tungsten target of 5 mm in which the electrons produce, in reason of Bremsstrahlung effect, high-energy photons, then a part of these high-energy photons produce, inside the tungsten itself, reactions (γ, n) and (γ, 2n), with thresholds, respectively, at 7 and 14 MeV.

In this way, starting from the acceleration of the electrons, we can have 10^6n/cm^2/s on our detectors.

To increase the temperature of fission chambers, in the way to observe and characterize the phenomenon of PD, a tube furnace was used, in all our experiments. All PD measurements were repeated for each chamber, spaced over time, to ensure that the phenomenon remain stable over time, in other words, to ensure that PD phenomenon does not bring any destructive effect on the fission chamber.

The electrical cables for each chamber are tested at several temperatures up to 650 °C and they did not record any PD during the time, around 1 h, in which they are exposed to temperature.

V. Pulse shape Characterization

The characterization of the electrical signals produced by the chambers, polarized to their nominal dc bias voltage (listed in Table II), was done for a large number (∼500–10 000) of accumulated signals, resulting either from neutron or PD pulses using the standard amplification.

A given experimental condition is therefore presented here using the average pulse waveform and a corresponding histogram of the pulse full-width at half maximum (FWHM) values from all the detected pulse signals.

A. Neutrons

Neutron detection signal characterization, as function of temperature and obtained from the three complete fission chambers (HTFC 1A, HTFC 1B, and HTFC 2) is shown in Fig. 4. Instead Table III shows the mean value and the standard deviation calculated from each histogram in Fig. 4.

In these experiments, the three fission chambers were polarized to their nominal bias voltage, shown in Table II, then they were subjected to neutron irradiation and gradually heated up to 650 °C. As seen in Fig. 4, the resulting pulses have a shape with very similar rise and fall times.

An increase in temperature causes an increase in the average value of the pulse FWHM. The data in Fig. 4 coupled with the values in Table III also show that, for the fission chamber with the smaller electrodes distance (HTFC 2), the average FWHM value is significantly reduced compared to the average FWHM values observed for the HTFC 1A and HTFC 1B. The gas pressure does not seem to significantly affect the signal shape in these fission chambers because no significant differences between histograms of HTFC 1A and HTFC 1B in Fig. 4 and in Table III are observed.

B. Partial Discharges

PD pulse characterization as a function of temperature and bias voltage, obtained from three different fission chambers

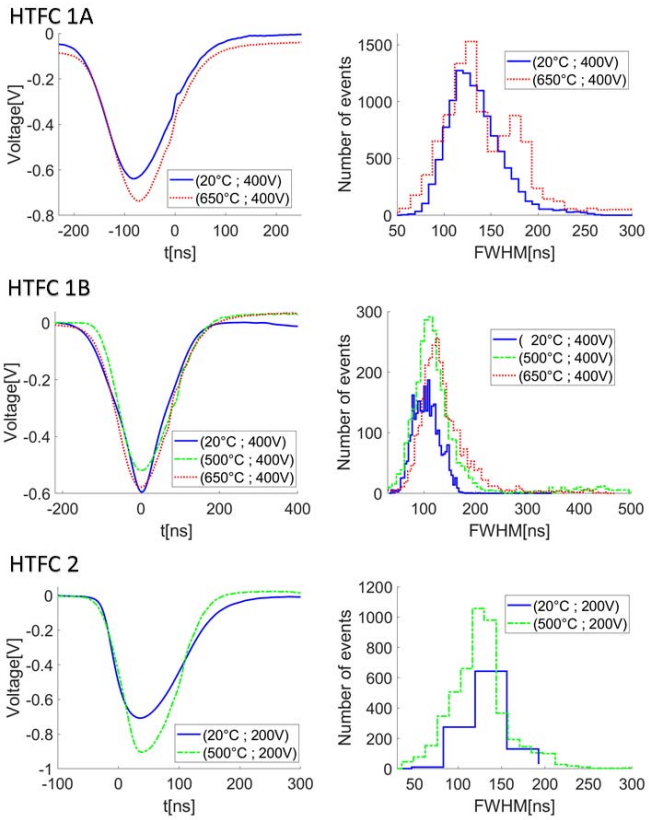

Fig. 4. Average neutron pulses (left) and histograms of the FWHM of more than 10 000 neutron pulses (right) for each fission chambers, recorded using a threshold of −450 mV, with a neutron flux of 10^6n/cm^2/s, generated by the Saphir facility described earlier; chambers were polarized to their nominal bias voltage and heated to different temperatures.

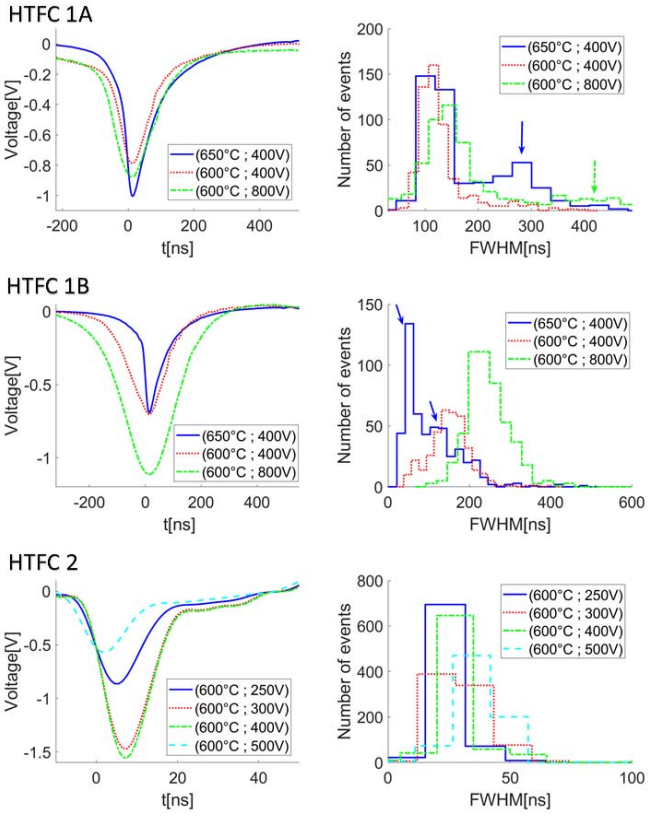

Fig. 5. Average PD pulses (left) and histogram of FWHM of PD pulses (right) for each fission chambers, recorded using a threshold of −450 mV, without a neutron source, polarized at different bias voltage and heated to different temperatures.

(HTFC 1A, HTFC 1B, and HTFC 2), is shown in Fig. 5. Instead Table IV shows the mean value and the standard deviation calculated from each histogram in Fig. 5.

The PD pulses, like neutron pulses, have a shape with very similar rise and fall times, which is due to the amplification circuit being the same.

In these experiments, the three fission chambers were polarized to different bias voltages without any source of neutron flux and were gradually heated up to 650 °C.

It can be noted again here that PDs were only observed for cases where fission chambers were heated above about 400 °C.

The average of the FWHM values was observed to be independent of the voltage or temperature, contrary to what was shown for the case of temperature variation in neutron pulses.

However, when the diameter of the fission chamber including its electrical connection section is reduced, the average FWHM value tends to decrease accordingly, as shown by comparing the results on HTFC 1A or HTFC 1B with HTFC 2 in Fig. 5 and in Table IV. It is anticipated that this result is due to the electrical discharge pathway being shorter for the fission chamber with the smaller diameter.

Fig. 5 also shows that while only one kind of PD seems to be present in HTFC 2, in HTFC 1A, and HTFC 1B when the product of temperature and voltage is increased beyond a certain limit, a new population of PD pulses with higher FWHM values appears; these are indicated by arrows in the right-hand plots.

TABLE IV

MEAN VALUES AND STANDARD DEVIATIONS OF DP PULSES FWHM

		μ[ns]	σ[ns]
HTFC 1A	(650°C ; 400V)	144	93
	(600°C ; 400V)	113	55
	(650°C ; 800V)	160	105
HTFC 1B	(650°C ; 400V)	87	70
	(600°C ; 400V)	133	52
	(650°C ; 800V)	220	59
HTFC 2	(600°C ; 250V)	11	5
	(600°C ; 300V)	15	9
	(600°C ; 400V)	15	8
	(600°C ; 500V)	21	7

Finally, the results for HTFC 2 in Fig. 5 coupled with the values in Table IV show that the PD pulses seem not to be affected by the voltage increase and they have a small standard deviation in FWHM histogram, while results on HTFC 1A and HTFC 1B in Fig. 5 and in Table IV show that, the PD pulses seem to be affected by increases of voltage or temperature, which increases their standard deviation in FWHM histogram.

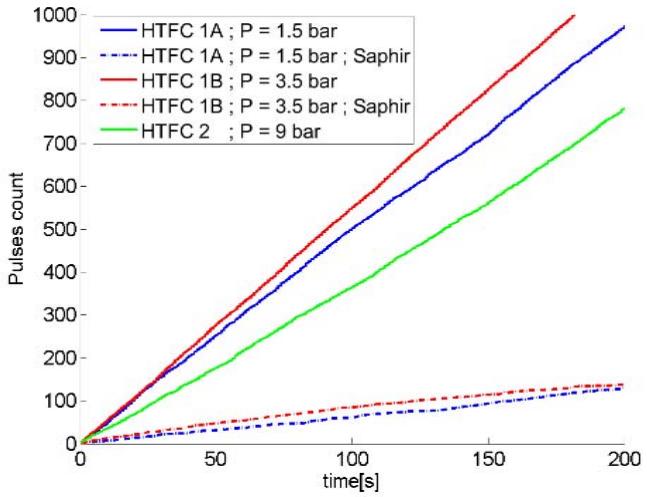

Fig. 6. PD pulse count as a function of time, recorded using a threshold of 450 mV, without neutron source, for chambers polarized to their nominal bias voltage and heated to 650 °C.

Fig. 6 shows the PD count as a function of time, without neutron source, for chambers polarized to their nominal bias voltage and heated at 650 °C. These pulses are acquired through the PING time-stamping acquisition system, developed at the French Atomic Commission (CEA) [13]. The larger fission chambers (HTFC 1A and HTFC 1B) have been tested twice: the first tests (solid lines) were made in a conventional laboratory, while the second tests (dashed lines) were made in the underground and shielded SAPHIR facility which is located at CEA in Saclay (France).

Fig. 6 shows, first, that the number of PD per second decreases with increasing filling pressure of the chambers. In addition, we can observe that when the tests are performed in Saphir facility, both large fission chambers have a very low PD count, and when the tests are performed in laboratory the PD count is significantly higher. The cause of very low PD count when the fission chambers were tested in the Saphir facility is the reduced flux of high-energy radiation of the Saphir facility compared to the ground level laboratory, without any radiation shield (per the mechanism presented in Fig. 1).

Therefore, if this reasoning is correct, then seed electron generation frequency is very small in the experiments performed in the Saphir facility compared to the experiments performed in a ground level laboratory, without any radiation shield; it is thus possible to explain the observed difference between dashed an solid lines in Fig. 6.

C. Neutron-Discharge Shape Comparison

In this section, the pulse characterizations discussed in Sections V-A and V-B are compared for each fission chamber.

Comparison of Fig. 4, in which the fission chambers were tested with neutron source and at high temperature, and Fig. 5, in which the fission chambers were tested at high temperature but without neutrons, shows that, in HTFC 2, neutron and PD pulses are well separated in terms of FWHM.

Comparison of Figs. 4 and 5 also shows that, in HTFC 1A and HTFC 1B, contrary to HTFC 2, neutron and PD pulses are very hard to separate because the voltage amplitude is quite similar and the FWHM histograms cover the same range of values in the two cases; it is thus possible that the observed PDs are located in different parts of the fission chambers with the smaller diameter (HTFC 2) than the larger ones.

VI. Discharge Localization: Methods and Results

To find the loci of occurrence of the PD, we have used three different methods: the first involves the use of a phase resolved pattern diagrams (PRPD) on fission chamber with the smaller diameter (HTFC 2), the second is based on the comparison between the PD observed in full neutron detectors (HTFC 1A and HTFC 1B) as opposed to the PD observed in the partial chambers, having no active zone but containing either both or only one of the electrical connectors (HTFC 3A, HTFC 3B, HTFC 4A, and HTFC 4B), which were constructed specifically to test for electrical discharges outside of the active zone of the real fission chambers and the third is based on the application of a temperature gradient on the large fission chamber (HTFC 1A).

A. PRPD Method

To perform this experiment, the HTFC 2 was placed in a tubular furnace at 650 °C without any neutron source, and connected to a 50-Hz ac voltage supply. An Omicron PD analyzer [19] was then used to create the pattern diagrams, as shown in Fig. 7. In the PRPD [20]–[23], PD events are displayed as points with vertical positions determined by the charge value and the horizontal positions determined by the timing with respect to applied voltage phase, which is indicated by the green sinusoidal curve. For multiple similar discharges, a color code is used for the display (red corresponding to multiple similar events and blue to few similar events), which creates the patterns seen in Fig. 7. The total average charge per cycle (Q_{IEC}) is shown in Fig. 7 (top right).

In this way, it is possible to characterize different PD phenomena according to the patterns obtained or according to the way in which the patterns vary by modifying the voltage or frequency.

In Fig. 7, PDs were characterized with increasing applied ac voltage and it is observed that an increase in voltage leads to a leftward movement of the resulting pattern.

The results on Fig. 7 support the hypothesis that an insulator is involved in the phenomenon because in positive side of voltage in Fig. 7, we observe that most of PDs appear long before the maximum voltage; this can occur when a dielectric is present in the system, leading to a charging effect. This charging effect is due to the deposition of charges on the insulator, which has the effect of decreasing the electric field between the electrodes in a given half cycle, with a corresponding increase in the effective electric field at an earlier time in the next half cycle, explaining why the PDs do not appear to correspond with the maximum of the voltage.

In Fig. 8, PDs were characterized with increasing the frequency of applied ac voltage and it was observed that an increase in frequency leads to an increase of occurrence of PDs over time.

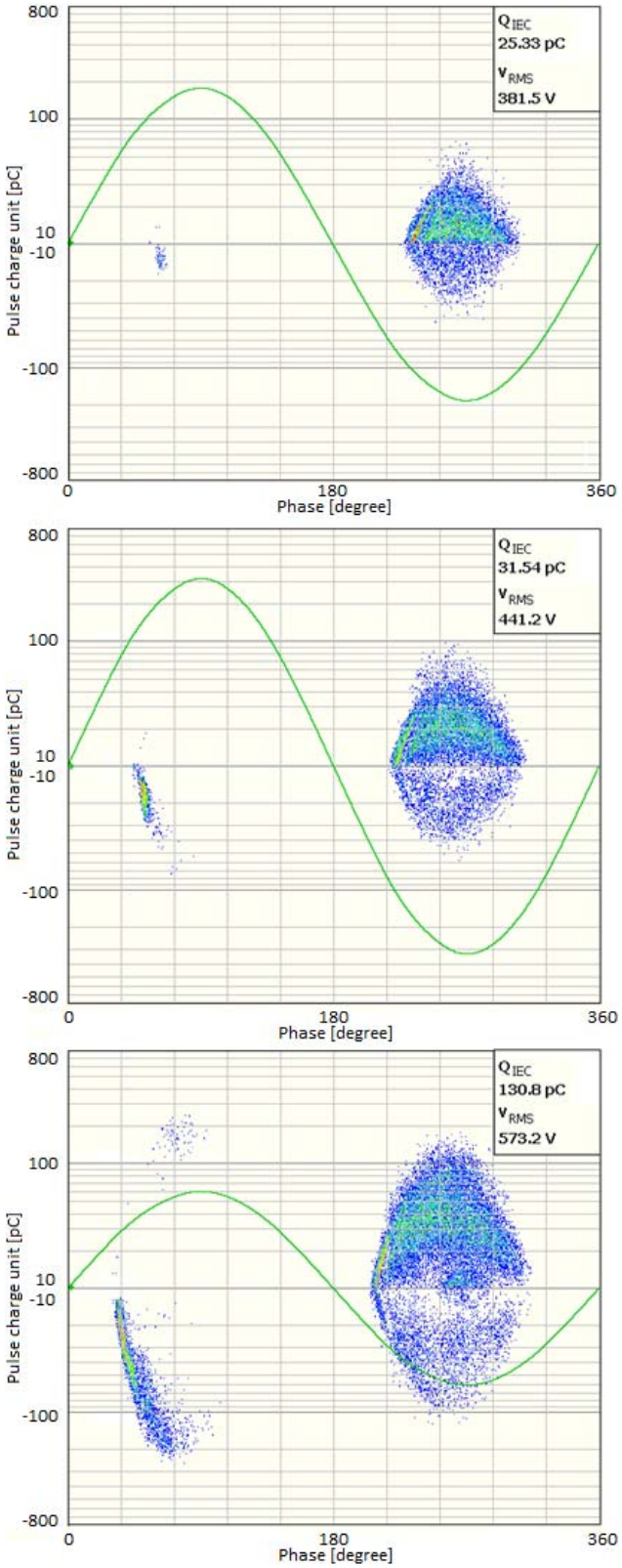

Fig. 7. PRPD patterns for PD in the presence of a progressive increase of alternative voltage to a frequency of 50 Hz and at 650 °C in HTFC 2; data were collected for a duration of 2 min for each measurement.

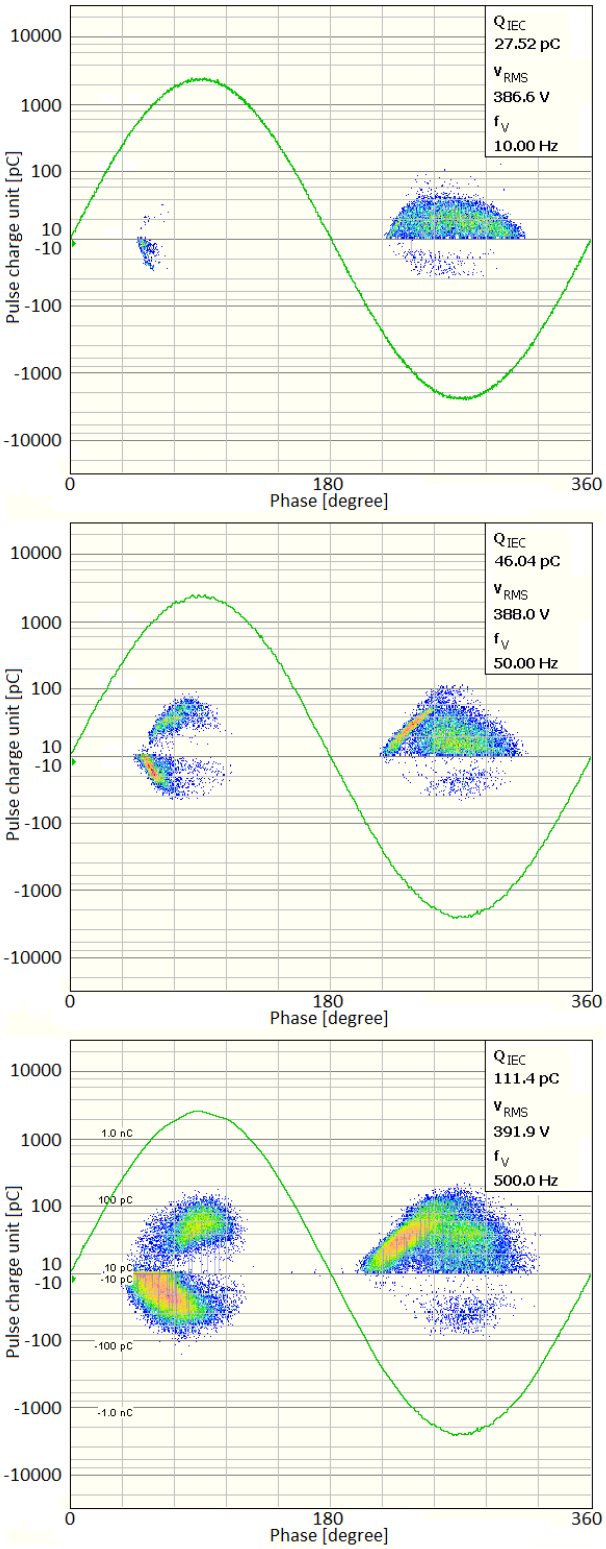

Fig. 8. PRPD patterns for PD in the presence of a progressive increase of frequency at the same V_{RMS} value and at 650 °C in HTFC 2; data were collected for duration of 2 min for each measurement.

Also in Fig. 8, the effects of frequency variation on the pattern modifications can be explained once again by the presence of a solid insulator because at low frequency the solid insulator has more time to lose the accumulated charges, so a low occurrence of PDs is observed, but at high frequency this time becomes too small and for this reason we observe a high occurrence of PDs.

Thanks to these results, it is proposed that an insulator is involved in the phenomenon [20], [21], and that the PDs are,

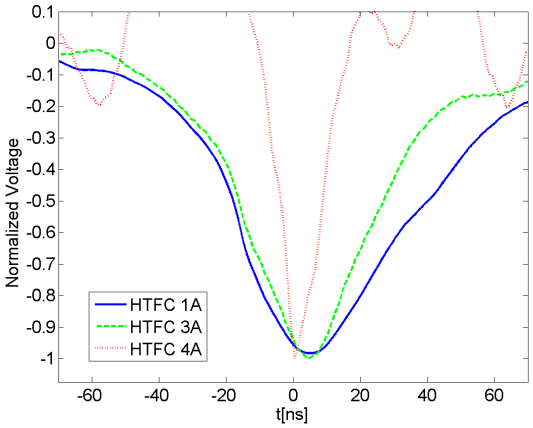

Fig. 9. Normalized average PD pulses of HTFC 1A (blue), HTFC 3A (green), and HTFC 4A (red) at 600 °C and 400 V, 1.5 bar; recorded using a threshold of −450 mV.

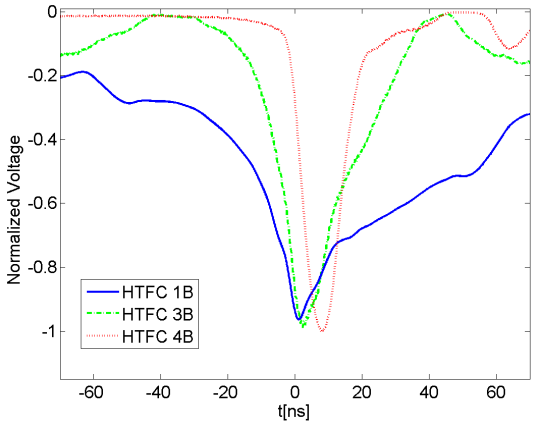

Fig. 10. Normalized average PD pulses of HTFC 1B (blue), HTFC 3B (green), and HTFC 4B (red) at 600 °C and 400 V, 3.5 bar; recorded using a threshold of −450 mV.

most likely, located in the chamber-cable electric connection zone, where most of the insulators are located, and not in the active part of the detector.

The fact that a heated insulator is involved in the formation of PDs is interesting. It is possible that charge transport on the surface of the insulators is involved in the formation of PDs through a mechanism which may involve the metal–insulator–gas triple point. Further work will investigate this mechanism.

B. Chamber-Cable Connection Tests

In order to further investigate the location of the PD observed in the fission chambers at high temperature, the four partial chambers shown in Fig. 3 (HTFC 3A, HTFC 3B, HTFC 4A, and HTFC 4B) were constructed by PHOTONIS and tested for PD activity.

None of the four partial chambers contained the active zone with cylindrical electrodes covered in fissile material. The first partial chamber type (HTFC 3A and HTFC 3B), contains both the chamber-cable electrical connection and the inner electrical connector which connects to the active zone in complete chambers.

The second partial chamber type (HTFC 4A and HTFC 4B) contains only the external electrical connector. Otherwise, all these four partial chambers are similar to the first two complete chambers shown in Fig. 3 (same diameter, materials, and geometry).

All four of these partial chambers and the complete chambers were tested at the same temperature and the average pulse shape and pulse count were compared.

Fig. 9 shows the normalized average pulse waveform for the three types of chamber (HTFC 1A, HTFC 3A, and HTFC 4A), with filling pressure of 1.5 bar, at 600 °C and 400-V bias voltage.

Fig. 10 shows the normalized average pulse waveform for the three types of chamber (HTFC 1B, HTFC 3B, and HTFC 4B), with filling pressure of 3.5 bar, at 600 °C and 400 V.

In Figs. 9 and 10, the FWHM of the signal pulses appears to increase from the case of chambers with only the external electrical connector (HTFC 4A and HTFC 4B) to the complete

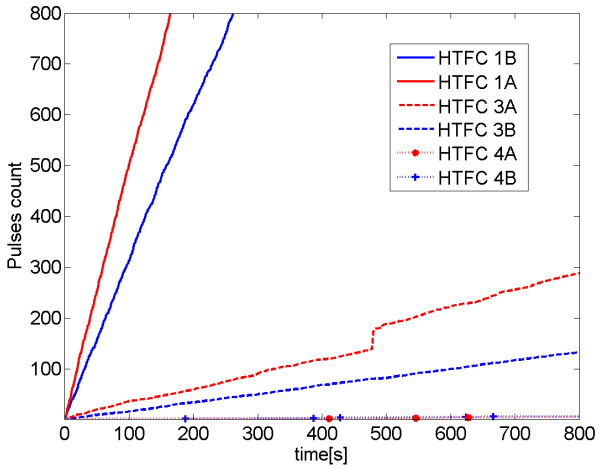

Fig. 11. Count of PD pulses as a function of time, without neutron source, at 600 °C and 400 V; recorded using a threshold of 450 mV.

fission chambers (HTFC 1A and HTFC 1B) and in both Figs. 9 and 10 the shape of green signals (two electrical connectors but no active zone) seem to be similar to the shape of blue signals (full chambers).

Fig. 11 shows the PD count as a function of time, acquired through the PING time-stamping acquisition system, developed at the CEA [13], where the slope of the curves gives us an idea of the number of PD per second over a period of time.

The partial chambers with only one of the two electrical connectors (HTFC 4A and HTFC 4B) have a very low PD count, the full chamber (HTFC 1A and HTFC 1B) has a high PD count, and the partial chambers with both connectors (HTFC 3A and HTFC 3B) have an intermediate PD count. These results therefore indicate that the problematic zone is the junction between the active zone of the complete chamber to the intermediate zone linking the active zone with the cable, and not the junction between the intermediate zone and the cable.

To conclude, the frequency of PDs is taken here as an indicator of the severity of the problem, and used to locate the problematic zone within the chamber. Further work will investigate the mechanisms leading to these results and seek to

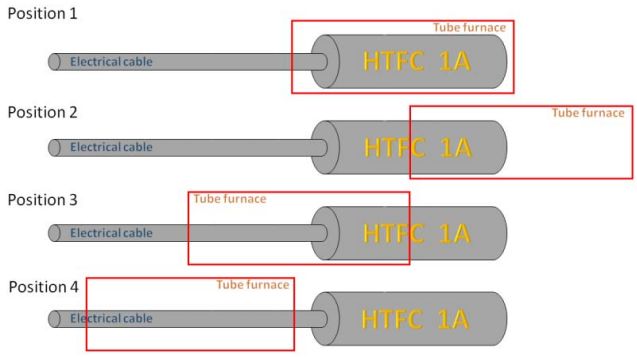

Fig. 12. Scheme of HTFC 1A positions in the tube furnace during the temperature gradient experiments.

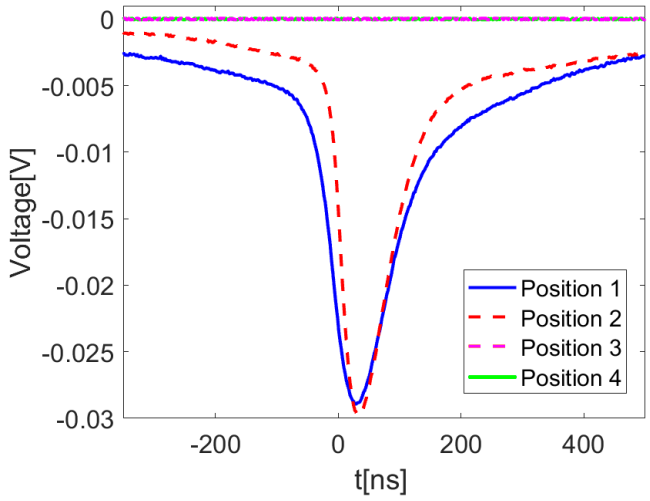

Fig. 13. Average signals resulting from PDs obtained for each configurations shown in Fig. 12, recorded using a threshold of −15 mV.

define design modifications to prevent PDs in fission chambers operating at high temperature.

C. Temperature Gradient Method

In order to investigate the temperature response of different zones within the fission chambers, the HTFC 1A was placed in a tube furnace at 650 °C in four different positions, as shown in Fig. 12, without any neutron source, and polarized to its nominal bias voltage. In this way, four different zones of the fission chamber were preferentially heated. These heated positions may be listed as follows:

1) the complete fission chamber with its electrical cable;
2) the cable-side half of the fission chamber with cable-chamber electrical connection and with its electrical cable;
3) the other half of the fission chamber without cable-chamber electrical connection and without electrical cable;
4) the electrical cable without the chamber.

Fig. 13 shows the average signals resulting from PDs, in HTFC 1A at 650 °C and its nominal bias voltage, obtained for each configuration depicted in Fig. 12.

PDs were only observed in the experiments for the case in which the cable-chamber electrical connection was heated, positions 1 and 2.

Thanks to these results it is proposed, once again, that an insulator is involved in the phenomenon, and that the PD are, most likely, located in the chamber-cable electric connection zone, where most of the insulators are located, and thus not in the active part of the detector.

VII. Conclusion

Results presented in this paper demonstrate first that it is difficult to discriminate between neutron detection signals and signals from PDs using FWHM analysis for the case of the larger fission chambers (HTFC 1A and HTFC 1B) but may be feasible for the fission chamber with smaller diameter and electrodes distance (HTFC 2).

The filling gas pressure was found not to significantly affect the PD pulse shape, while some broadening of the pulse signals was observed with increasing temperature.

A change in the ambient ionizing radiation present in the geographic location of the experiments (whether in a ground level laboratory without any radiation shield or in a shielded underground facility) can completely change the PD count when using the same fission chamber.

Tests using an ac power supply and PD analyzer indicate that the mechanism leading to PDs in the chambers involves an insulator.

Results on PD pulse localization showed that the majority of the PDs are located near the electrical connection linking the active zone of the chamber with the intermediate zone, and therefore likely involve the alumina insulator in this connector.

In addition, we show that the number of PD per second decreases with increasing filling pressure of the chambers.

Following these results further tests will be performed to better understand the problematic zone of the chambers and the specific mechanism responsible for these discharges.

In addition, higher filling pressure or different gases will be tested to reduce or eliminate these discharges. A better understanding of the mechanism should then lead to the definition of design changes for the elimination of the problem of PDs in HTFCs.

References

[1] G. F. Knoll, *Radiation Detection and Measurement*. New York, NY, USA: Wiley, 1989.

[2] S. Andriamonje *et al.*, "New neutron detector based on micromegas technology for ADS projects," *Nucl. Instrum. Methods Phys. Res. A, Accel. Spectrom. Detect. Assoc. Equip.*, vol. 562, no. 2, pp. 755–759, 2006.

[3] B. Geslot *et al.*, "Development and manufacturing of special fission chambers for in-core measurement requirements in nuclear reactors," in *Proc. 1st Int. Conf. Advancements Nucl. Instrum. Meas. Methods Appl. (ANIMMA)*, Marseille, France, Jun. 2009, pp. 1–4.

[4] C. Jammes, B. Geslot, and G. Imel, "Advantage of the area-ratio pulsed neutron source technique for ADS reactivity calibration," *Nucl. Instrum. Methods Phys. Res. A, Accel. Spectrom. Detect. Assoc. Equip.*, vol. 562, no. 2, pp. 778–784, 2006.

[5] C. Jammes, B. Geslot, R. Rosa, G. Imel, and P. Fougeras, "Comparison of reactivity estimations obtained from rod-drop and pulsed neutron source experiments," *Ann. Nucl. Energy*, vol. 32, no. 10, pp. 1131–1145, 2005.

[6] C. Jammes, P. Filliatre, B. Geslot, T. Domenech, and S. Normand, "Assessment of the high temperature fission chamber technology for the French fast reactor program," *IEEE Trans. Nucl. Sci.*, vol. 59, no. 4, pp. 1351–1359, Aug. 2012.

[7] J. P. Trapp, S. Haan, and L. Martin, "High temperature fission chambers. State-of-the-art," in *Proc. Spec. Meeting In-Core Instrum. Reactor Core Assessment*, Mito, Japan, 1996, pp. 191–202.

[8] H. Hamrita, C. Jammes, G. Galli, and F. Laine, "Rejection of partial-discharge-induced pulses in fission chambers designed for sodium-cooled fast reactors," *Nucl. Instrum. Methods Phys. Res. A, Accel. Spectrom. Detect. Assoc. Equip.*, vol. 848, no. 11, pp. 109–113, 2017, doi: 10.1016/j.nima.2016.11.055.

[9] J. F. Miller, "Fission chambers," in *Wiley Encyclopedia of Electrical and Electronics Engineering*. Hoboken, NJ, USA: Wiley, 2015, doi: 10.1002/047134608X.W5203.pub2.

[10] C. Jammes *et al.*, "Progress in the development of the neutron flux monitoring system of the French GEN-IV SFR: Simulations and experimental validations," in *Proc. ANIMMA*, Apr. 2015, pp. 1–8.

[11] C. Blandin, G. Bignan, A. Lebrun, O. Poujade, and S. Breaud, "Development and modeling of neutron detectors for in-core measurement requirements in nuclear reactors," in *Proc. 10th Int. Symp. Reactor Dosimetry*, 1999, pp. 803–810.

[12] C. Jammes *et al.*, "Research activities in fission chamber modeling in support of the nuclear energy industry," *IEEE Trans. Nucl. Sci.*, vol. 57, no. 6, pp. 3678–3682, Dec. 2010.

[13] S. Normand *et al.*, "PING for nuclear measurements: First results," *IEEE Trans. Nucl. Sci.*, vol. 59, no. 4, pp. 1232–1236, Aug. 2012.

[14] F. Carrel *et al.*, "Characterization of old nuclear waste packages coupling photon activation analysis and complementary non-destructive techniques," *IEEE Trans. Nucl. Sci.*, vol. 61, no. 4, pp. 2137–2143, Aug. 2014.

[15] A. Sari, F. Carrel, F. Lainé, and A. Lyoussi, "Neutron interrogation of actinides with a 17 MeV electron accelerator and first results from photon and neutron interrogation non-simultaneous measurements combination," *Nucl. Instrum. Methods Phys. Res. B, Beam Interact. Mater. At.*, vol. 312, pp. 30–35, Oct. 2013.

[16] A. Sari, F. Carrel, F. Lainé, and A. Lyoussi, "Design of a neutron interrogation cell based on an electron accelerator and performance assessment on 220 liter nuclear waste mock-up drums," *IEEE Trans. Nucl. Sci.*, vol. 61, no. 4, pp. 2144–2148, Aug. 2014.

[17] A. Sari *et al.*, "Characterization of the photoneutron flux emitted by an electron accelerator using an activation detector," *IEEE Trans. Nucl. Sci.*, vol. 60, no. 2, pp. 693–700, Apr. 2013.

[18] A. Sari, F. Carrel, C. Jouanne, A. Lyoussi, and O. Petit, "Optimization of the photoneutron flux emitted by an electron accelerator for neutron interrogation applications using MCNPX and TRIPOLI-4 Monte Carlo codes," in *Proc. IPAC*, 2013, pp. 3630–3632.

[19] *OMICRON Energy Solutions GmbH*, Berlin, Germany, OMICRON, 1984.

[20] C. Hudon and M. Belec, "Partial discharge signal interpretation for generator diagnostics," *IEEE Trans. Dielectr. Electr. Insul.*, vol. 12, no. 2, pp. 297–319, Apr. 2005.

[21] H. Illias, T. S. Yuan, A. H. A. Bakar, H. Mokhlis, G. Chen, and P. L. Lewin, "Partial discharge patterns in high voltage insulation," in *Proc. IEEE Int. Conf. Power Energy (PECon)*, Kota Kinabalu, Malaysia, Dec. 2012, pp. 750–755.

[22] R. Altenburger, C. Heitz, and J. Timmer, "Analysis of phase-resolved partial discharge patterns of voids based on a stochastic process approach," *J. Phys. D, Appl. Phys.*, vol. 35, no. 11, p. 1149, 2002.

[23] A. Müller, M. Beltle, and S. Tenbohlen, "Automated PRPD pattern analysis using image recognition," *Int. J. Elect. Eng. Inform.*, vol. 4, no. 3, pp. 483–494, 2012.

[24] J. M. Meek and J. D. Craggs, *Electrical Breakdown of Gases*. Hoboken, NJ, USA: Wiley, 1978.

[25] E. Badareu and I. Popescu, "Gaz ionisés. Décharges electriques dans le gaz," *J. Plasma Phys.*, p. 336, 1969.

[26] A. E. D. Heylen, "Sparking formulae for very high-voltage paschen characteristics of gases," *IEEE Elect. Insul. Mag.*, vol. 22, no. 3, pp. 25–35, May/Jun. 2006.